

# Deformation, structural changes and damage evolution in nanotwinned copper under repeated frictional contact sliding

A. Singh<sup>a</sup>, M. Dao<sup>a,\*</sup>, L. Lu<sup>b</sup>, S. Suresh<sup>a</sup>

<sup>a</sup> Department of Materials Science and Engineering, Massachusetts Institute of Technology, Cambridge, MA 02139, USA

<sup>b</sup> Shenyang National Laboratory for Materials Science, Institute of Metal Research, Chinese Academy of Sciences, 72 Wenhua Road, Shenyang 110016, People's Republic of China

Received 1 July 2011; received in revised form 9 August 2011; accepted 12 August 2011

## Abstract

Nanotwinned metals have the potential for use as structural materials by virtue of having a combination of high strength as well as reasonable ductility and damage tolerance. In the current study, the tribological response of nanotwinned copper has been characterized under conditions of repeated frictional sliding contact with a conical tip diamond indenter. Pure ultrafine-grained copper specimens of fixed grain size (~450 nm), but with three different structural conditions involving relatively high, medium and negligible concentrations of nanotwins, were studied. The effects of twin density and number of repetitions of sliding cycles on the evolution of friction and material pile-up around the diamond indenter were studied quantitatively by depth-sensing instrumented frictional sliding. Cross-sectional focused ion beam and scanning electron microscopy observations were used to systematically monitor deformation-induced structural changes as a function of the number of passes of repeated frictional sliding. Nanoindentation tests at the base of the sliding tracks coupled with large-deformation finite-element modeling simulations were used to assess local gradients in mechanical properties and deformation around the indenter track. The results indicate that friction evolution as well as local mechanical response is more strongly influenced by local structure evolution during repeated sliding than by the initial structure. An increase in twin density is found to result in smaller pile-up height and friction coefficient. Compared to the low-density nanotwinned metal, high-density nanotwinned copper showed significantly higher resistance to surface damage and structural changes, after the initial scratch. However with an increase in the number of sliding passes, the friction coefficient and rate of increase of pile up for all specimens acquire a steady value which does not change significantly in subsequent scratch passes. The frictional sliding experiments also lead to the striking result that copper specimens with both a high and low density of nanotwins eventually converge to a similar microstructure underneath the indenter after repeated tribological deformation. This trend strongly mirrors the well-known steady-state response of microcrystalline copper subjected to uniaxial cyclic loading. General perspectives on contact fatigue response of nanotwinned copper are developed on the basis of these new findings.

© 2011 Acta Materialia Inc. Published by Elsevier Ltd. All rights reserved.

**Keywords:** Nanoscale twins; Contact fatigue; Wear resistance; Microstructure evolution; Nanocrystalline copper

## 1. Introduction

Materials employed in most structural applications need to possess a combination of desirable mechanical properties such as high strength, ductility, wear and corrosion resistance, and damage tolerance under monotonic and

cyclic loading. Nanograined (NG) materials, despite their high strength and wear resistance, suffer from limited ductility [1], fatigue crack growth resistance [2] and fracture toughness [3,4]. Nanotwinned (NT) metals have been shown to possess some appealing properties in that they demonstrate high strength with an increase in twin density. The increase in yield strength with increasing twin density (or decreasing twin lamellar spacing) has been shown to follow the Hall–Petch-type relationship for a variety of

\* Corresponding author. Tel.: +1 617 253 2100.

E-mail address: [mingdao@mit.edu](mailto:mingdao@mit.edu) (M. Dao).

face-centered cubic (fcc) metal systems including stainless steel [5], Ni–Co alloys [6] and electrodeposited [7] and magnetron-sputtered Cu [8]. Tensile studies of NT Cu having a controlled density of initially coherent nanoscale twins inside ultrafine grains ( $\sim 450$  nm grain size) have also exhibited reasonable ductility [9–11]. Recent experiments [12] further reveal that NT Cu exhibits high strength and reasonable ductility while simultaneously preserving fracture toughness and resistance to fatigue crack growth. These beneficial attributes have been ascribed to twin boundaries (TBs) that obstruct dislocation motion while facilitating an ample reserve of dislocations in each grain by acting as both sources and sinks for dislocations [10,13–15]. As a result, NT metals promote greater plasticity than their nanocrystalline counterparts. In addition, the strain-rate sensitivity, activation volume and hardness of ultrafine-grained (UFG) Cu (with a grain size in the 100–1000 nm range) with nanoscale twins are found to be similar to those of NG Cu strengthened by grain refinement, if the nanoscale twin lamellar spacing in the former matches the analogous grain size for the NG Cu [11,16,17]. Furthermore, increasing the twin density does not adversely affect the electrical conductivity and electromigration properties of Cu, unlike decreasing the grain size into the nano regime [18].

In addition to high strength, ductility and damage tolerance, good tribological properties are indispensable for many engineering applications involving both structural components and surface coatings. The effect that the introduction of nanotwins in UFG Cu will have on the tribological response has not been systematically studied. In fact, very few quantitative experimental studies of continuous, depth-sensing frictional sliding contact have been reported for any material system along with quantitative micromechanical analysis of contact deformation, damage and structure evolution [19,20]. Only a few mechanical cyclic loading studies are available on NT materials and they reveal enhanced mechanical stability of TBs [21]. For example, multilayer Cu/Cu specimens with nanoscale twins produced by magnetron sputtering have been shown to exhibit considerable microstructural stability and hardness retention even under fatigue loading and indentation [21,22]. Although wear damage studies have been performed on a variety of micro- and nanograined materials used in bulk and small-volume structures [20–27], no experimental results are available for NT metals subjected to repeated sliding contact and damage.

A key issue with frictional sliding experiments is the possibility that the microstructure may not remain stable in the vicinity of the scratch surface after frictional sliding. Most wear studies on coarse-grained materials have shown that as a result of large stresses and plastic strains imposed by the sliding process, the microstructure of the region close to the scratch surface is severely altered with the progression of sliding. This deformation-induced microstructure change is instrumental in affecting the subsequent wear response of metals under repeated sliding. The surface

“tribolayer” so formed can have structural, substructural and chemical characteristics completely different from the original material [23]. The substructure has often been compared to that observed in metals and alloys after severe plastic deformation (SPD) processes where the structure size evolution is dependent on the stacking fault energy, applied stress, test conditions and temperature [24,25]. Frictional sliding studies on NG Ni found that the microstructure did not remain stable with sliding and significant grain coarsening occurred in the sliding track [18]. Grain coarsening accompanied by hardening has been observed for Ni–W alloys with an initial grain size ranging from 3 to 10 nm to a final grain size close to 20 nm under contact sliding, whereas a negligible change in grain size was observed for initial grain sizes greater than 10 nm [26].

The present work constitutes a depth-sensing instrumented study in which the effect of twin density on the friction coefficient as a function of number of repeated contact sliding passes has been investigated. Pile-up of material around the indenter was also investigated for all the specimens with different twin densities. Microstructure evolution during repeated frictional sliding has been observed and hardness evolution has been quantified by recourse to quantitative indentation tests along the wear tracks performed at periodic intervals. We supplement measurements with dimensional analysis and large deformation finite-element method (FEM) computational simulations. The mechanics of indentation on a grooved surface has also been modeled, and has been used to extract the flow strength in the deformation-affected zone for all the specimens at different pass numbers. Through such experiments and computations, we demonstrate the effects of the introduction of coherent nanoscale twins in UFG Cu on the sliding contact fatigue characteristics. Earlier work on constant-amplitude strain-controlled fatigue has shown that pure fcc metals under repeated uniaxial loading attain a characteristic steady state saturation flow stress and microstructure that is dependent on the strain, strain rate and temperature [27,28]. We discuss possible mechanisms underlying the similarities and differences between strain-controlled uniaxial fatigue and repeated frictional sliding.

## 2. Materials and methods

### 2.1. Materials

High-purity Cu specimens (with in-plane dimensions of  $20 \text{ mm} \times 10 \text{ mm}$ , and  $100 \mu\text{m}$  thick) with nanoscale growth twin lamellae were synthesized by means of pulsed electrodeposition from an electrolyte of  $\text{CuSO}_4$ . The as-deposited NT Cu specimen has roughly equiaxed grains (with an average grain size of 400–500 nm), with a high concentration of coherent growth TBs. A Cu specimen with an average twin lamellar spacing of  $15 \pm 7 \text{ nm}$  (hereafter referred to as HDNT Cu, i.e. high-density nanotwinned Cu) and one with an average twin lamellar spacing of  $85 \pm 15 \text{ nm}$

(hereafter referred to as LDNT Cu, i.e. low-density nanotwinned Cu) were selected for detailed sliding contact fatigue studies. For comparison as a control condition, a UFG Cu specimen of the same grain size, but with essentially no twins, was produced from the same electrolyte by means of direct current electrodeposition. The density of the as-deposited specimens was ascertained to be  $8.93 \pm 0.03 \text{ g cm}^{-3}$ . The purity of the as-deposited Cu was measured to be higher than 99.998 at.% with less than 8 ppm S content. Hydrogen and oxygen levels were determined by chemical analysis to be less than 15 and 20 ppm, respectively. These same test materials and control material have been the subject of extensive prior investigations of strength, ductility and damage tolerance, and their structures have been characterized thoroughly by electron microscopy [7,9–12]. The specimen preparation procedure and the structural characteristics of the as-deposited NT Cu are described elsewhere [7]. The specimens were glued onto steel specimen holders using cyanoacrylate glue for the frictional sliding experiments.

## 2.2. Experimental procedure

An instrumented nanoindenter, NanoTest™ (Micromaterials, Wrexham, UK), was used to conduct all sliding contact fatigue experiments. Force transducers mounted on either side of the indenter tip monitored tangential loads generated during scratch experiments, and a conical diamond tip ( $70.3^\circ$  tip half angle and  $2 \mu\text{m}$  tip radius) was used in each test. Tips were replaced after every experiment to avoid material transfer between specimens and to ensure that variations in tip radius due to severe deformation were minimized among experiments. Initial contact was made between polished specimens (thoroughly cleaned in an ultrasonic ethanol bath) and the indenter tip, after which a prescribed normal load was applied as the specimen stage was displaced at a constant rate of  $5 \mu\text{m s}^{-1}$ . The normal load was ramped up to its maximum value of 500 mN over the first  $50 \mu\text{m}$  of stage motion, and remained constant thereafter. A  $500 \mu\text{m}$  scratch at the maximum normal load was then introduced, followed by a  $15 \mu\text{m}$  tip retraction from the surface. The sample stage was subsequently returned to its initial position, and the scratch was repeated in this unidirectional fashion. Fig. 1 illustrates this repeated contact sliding procedure. Through this method, 1, 10, 17, 20, 30, 34, 40, 50, 60, 66, 70, 80, 82, 90 and 98 sliding cycles were imposed in seven different tracks which were sufficiently spaced apart so that the possibility of interaction between the stress-induced deformation zones of different scratch tracks is eliminated. Normal and tangential loads were acquired throughout the entire length of the scratch.

In order to investigate hardness evolution under repeated sliding, indentations were performed on the seven scratch tracks using instrumented nanoindentation. The diamond indenter tip was conical with a tip half-angle of  $70.3^\circ$  and a tip radius of  $2 \mu\text{m}$ . The indentations were depth-controlled and the load required to reach a depth

of  $1 \mu\text{m}$  was recorded. All these indentations were performed at a fixed loading rate of  $10 \text{ mN s}^{-1}$ .

After the experiment, a series of at least 30 cross-sectional residual profiles were obtained over the steady-state regime by using a Tencor P10 profilometer (KLA-Tencor, San Jose, CA, USA). The profilometer was equipped with a conical diamond probe that had an apex angle of  $45^\circ$  and a tip radius of  $2 \mu\text{m}$ . From these profiles the pile-up height for all of the specimens for all the pass numbers was determined.

In order to assess deformation-induced microstructure changes, specimens were ground on a 320 grit SiC paper (followed by a 1000 grit SiC paper) to reach the centre of the length of the sliding tracks with continuous cooling maintained throughout grinding process. The cross-section of the scratch was subsequently polished by focused ion beam (FIB). The cross-section was observed by high-resolution scanning electron microscopy (SEM) using an FEI Quanta 600 microscope (FEI Company, Hillsboro, Oregon, USA).

## 3. Results

### 3.1. Friction coefficient

Fig. 2 shows the evolution of total friction coefficient at a normal indentation load of 500 mN, as a function of the number of unidirectional scratch passes in all three materials. The total friction coefficient decreases as the number of sliding passes increases. A “steady-state” friction coefficient is reached after approximately 80 passes. It is also evident from Fig. 2 that increasing the twin density leads to a lower value of the total friction coefficient.

### 3.2. Pile-up height

The ploughing of the indenter over the specimens leads to a pile-up of material around the scratch groove. From the instrumented depth-sensing frictional sliding experiments, the height of the pile-up as a measure of deformation and damage is plotted as a function of pass number (Fig. 3). The incremental increase in pile-up height after each pass decreases as the pass number increases for all the specimens, and it eventually reaches a constant rate after about 66 passes. LDNT Cu has the lowest pile-up for all pass numbers, and the pile-up increase is higher for the materials with the lower twin density (i.e. lower strength). However, eventually all three specimens show similar rates of steady-state pile-up height increase per each new sliding pass.

### 3.3. Structure evolution

The deformation-affected zone for all the specimens after the 1st and 82nd (final) passes was examined under SEM after FIB sectioning. Fig. 4 shows a comparison of the deformation-induced structure change after the 1st

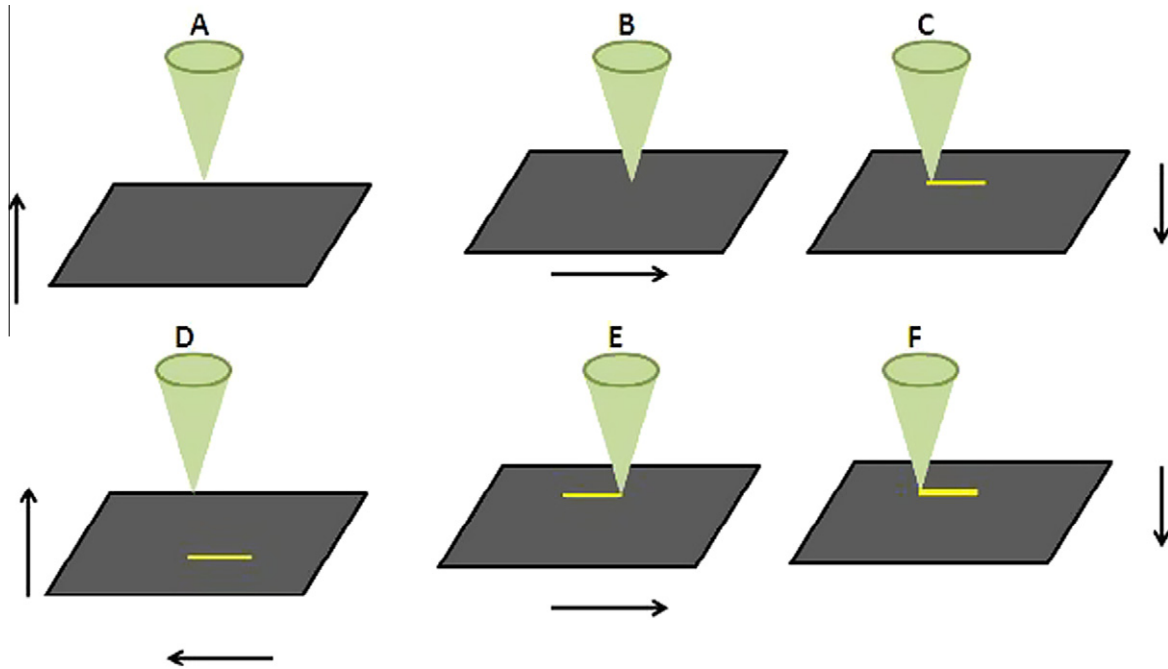


Fig. 1. A schematic drawing of the repeated contact sliding experiment. (A) Sample stage is brought close to the tip. (B) Sample stage is moved to the right to make a scratch. (C) Sample stage is moved away from the tip. (D) Sample stage is restored to its original position and brought in contact with the tip to repeat sliding at the same position. (E) Sample stage is moved to make another scratch along the same track. (F) Two cycles of sliding completed.

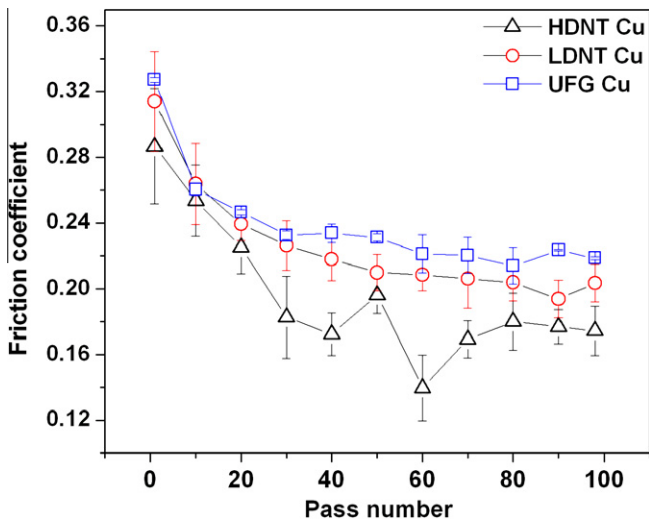


Fig. 2. Total friction coefficient as a function of sliding pass number for HDNT, LDNT and UFG Cu. The friction coefficient decreases with increasing passes and eventually reaches a plateau value for each case. The friction coefficient decreases with an increase in twin density.

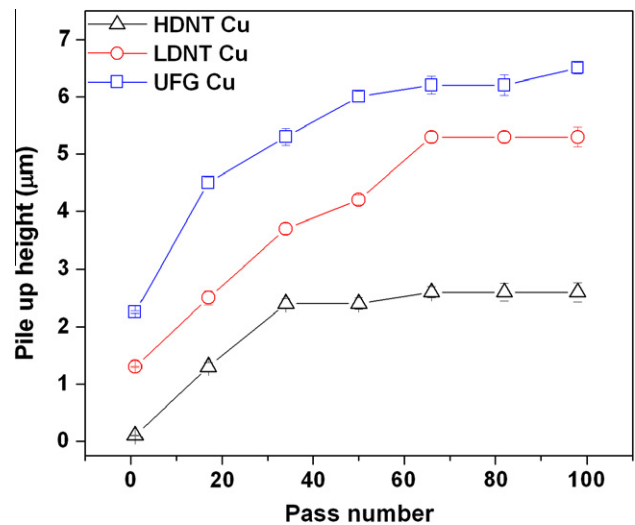


Fig. 3. Pile-up height for HDNT, LDNT and UFG Cu as a function of sliding pass number, showing that pile-up is a decreasing function of twin density.

sliding cycle for the HDNT and LDNT Cu specimens (with essentially the same initial average grain size). Here, one observes a significant microstructure change even after just one pass of contact sliding for the LDNT Cu specimen. The micrograph for the LDNT specimen shows considerable grain refinement close to the surface of the scratch. As the distance beneath the contact surface increases, the changes to structure from deformation progressively diminish and the structure appears coarser as the depth

from the surface increases. Fig. 5 shows grain size distribution for the LDNT and HDNT specimens after the 1st scratch. The deformation-induced area can be broadly divided into two zones (also see Figs. 10 and 11). The first zone for LDNT Cu has an average grain size of about 80 nm and extends up to a depth of 0.7 μm below the surface of the scratch. However, the minimum grain size in the first zone is as low as 30 nm for some grains near the scratch surface. The second zone has an average grain size of 200 nm and extends up to a depth of 2.5 μm below the

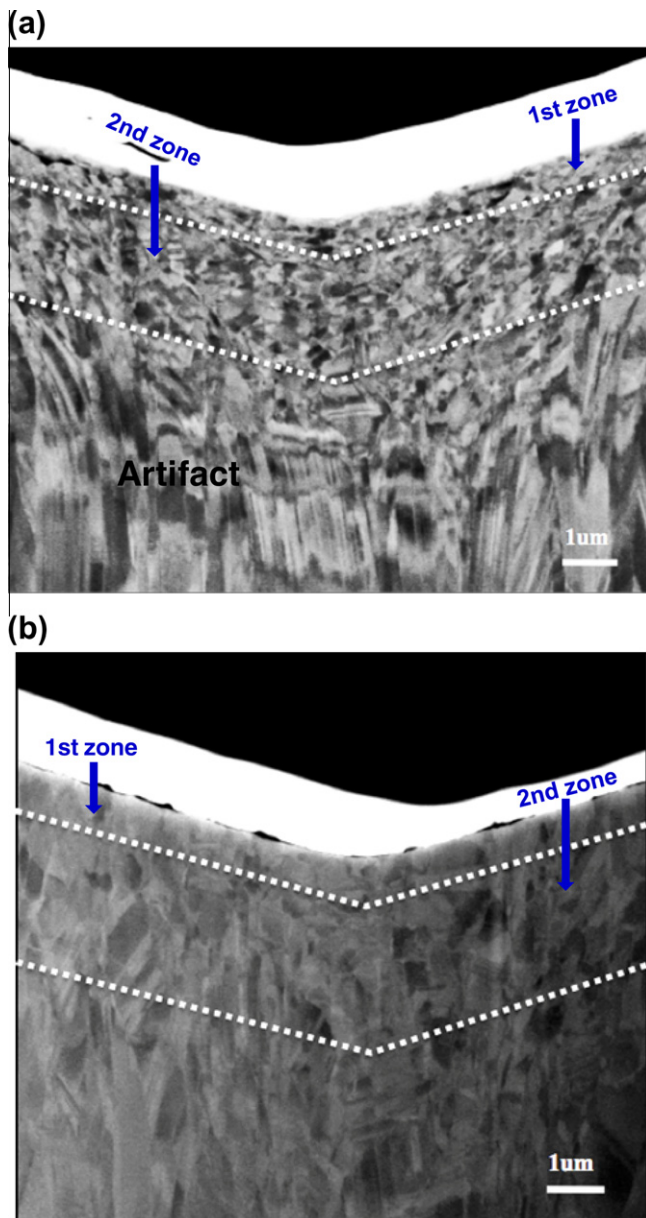


Fig. 4. SEM images of (a) LDNT Cu and (b) HDNT Cu specimens showing deformation-induced microstructure changes in the vicinity of the scratch surface after the 1st pass of frictional contact sliding. Grain refinement near the surface can be observed in LDNT Cu while no apparent change in the grain size for HDNT Cu is observed in spite of the high strains induced by the frictional sliding process.

first zone. No obvious grain size change can be identified for the HDNT Cu specimen after the 1st pass. The original microstructure with grain size of 400–500 nm consisting of high-density nanoscale twins is retained (also see Fig. 11 below).

As can be seen in Figs. 6 and 7, repeated sliding over 82 passes leads to drastic structure changes for both LDNT and HDNT Cu. It is evident from the grain size change close to the surface in LDNT Cu that the deformation-affected zone is much larger than that after the 1st pass of sliding. HDNT Cu, whose grain size is largely unaffected

after the 1st pass, exhibits a similar final microstructure compared to LDNT Cu after 82 passes of sliding. The deformed area for both the specimens can be broadly classified into three zones beyond which the original microstructure is preserved. The first zone has an average grain size of  $\sim 45$  nm for LDNT Cu and  $\sim 40$  nm for HDNT Cu, and extends up to a depth of  $1.4 \mu\text{m}$  below the scratch surface. The smallest grain size along the scratch surface in the first zone is found to be  $< 30$  nm. The second zone has an average grain size of  $\sim 120$  and  $\sim 110$  nm for LDNT and HDNT Cu, respectively, and extends up to a depth of  $1.8 \mu\text{m}$  below the first zone. Beyond the second zone, there exists a large region in which LDNT and HDNT Cu have an average grain size of  $\sim 280$  and  $\sim 305$  nm, respectively.

### 3.4. Evolution of flow strength

Analysis of the load ( $P$ ) vs. displacement ( $h$ ) curves obtained after indenting the grooved surface of the scratch led to the extraction of estimated surface yield strength of the HDNT and LDNT Cu as a function of the number of sliding passes using the procedure described in the Appendix. The deformation-induced flow stress change in all the specimens is plotted as a function of the number of sliding passes in Fig. 8. The evolution of flow stress in the vicinity of the scratch surface correlates well with the observed deformation-induced microstructure changes shown earlier. It can be seen that HDNT Cu exhibits its peak yield stress in the first pass, and with an increase in the number of sliding passes, the material in the vicinity of the scratch surface softens. LDNT Cu, on the other hand, displays low stress in the first cycle but undergoes a monotonic increase in flow stress and eventually the flow stress values of both HDNT and LDNT Cu approach a common value.

## 4. Discussion

A wear-resistant material should exhibit minimal pile-up height after being scratched by an indenter. An increase in twin density (which also concomitantly elevates material flow strength) leads to a reduction in pile-up height (Fig. 2). The differential change in pile-up height vs. pass number also progressively diminishes with an increase in pass number. Eventually the rate of pile-up height change appears to reach a steady state for all the specimens after 82 passes (Fig. 3). This trend is consistent with the repeated contact sliding studies of commercial stainless steel [29] which showed that the depth of penetration per cycle reaches a constant value after multiple cycles following the initial transient regime. Moreover, the microstructure of the tribolayer for LDNT and HDNT Cu in our work have been shown to be very similar after 82 passes of sliding. The convergence of the rate of pile-up height with respect to the pass numbers for LDNT and HDNT Cu further substantiates the earlier observation [30] that the wear response is significantly affected by the nature of the

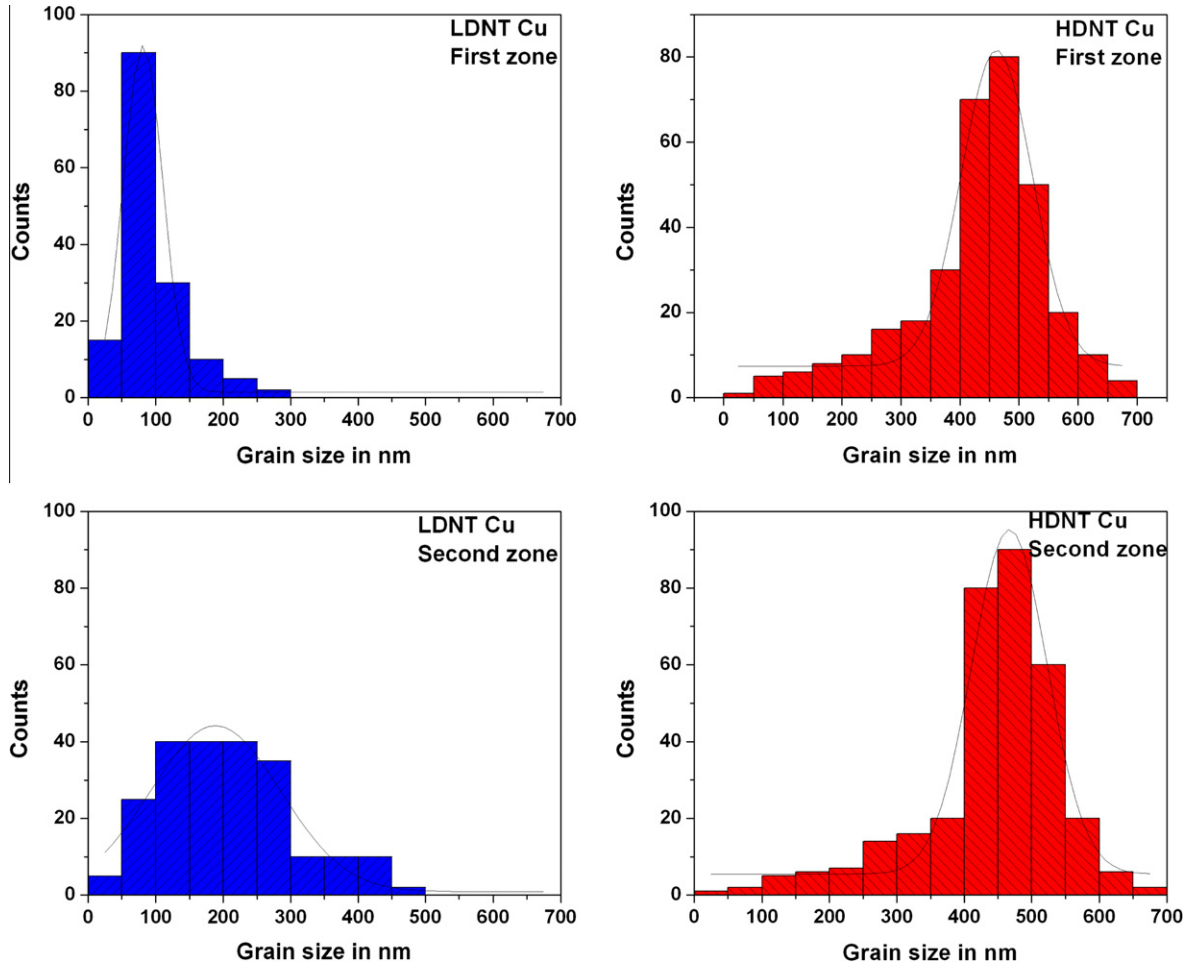


Fig. 5. Grain size distribution of LDNT and HDNT specimens just below the contact surface of the specimen after the 1st pass of sliding. There is little change in the microstructure below the HDNT specimen. Significant grain refinement is observed in the vicinity of the scratch for the LDNT specimen.

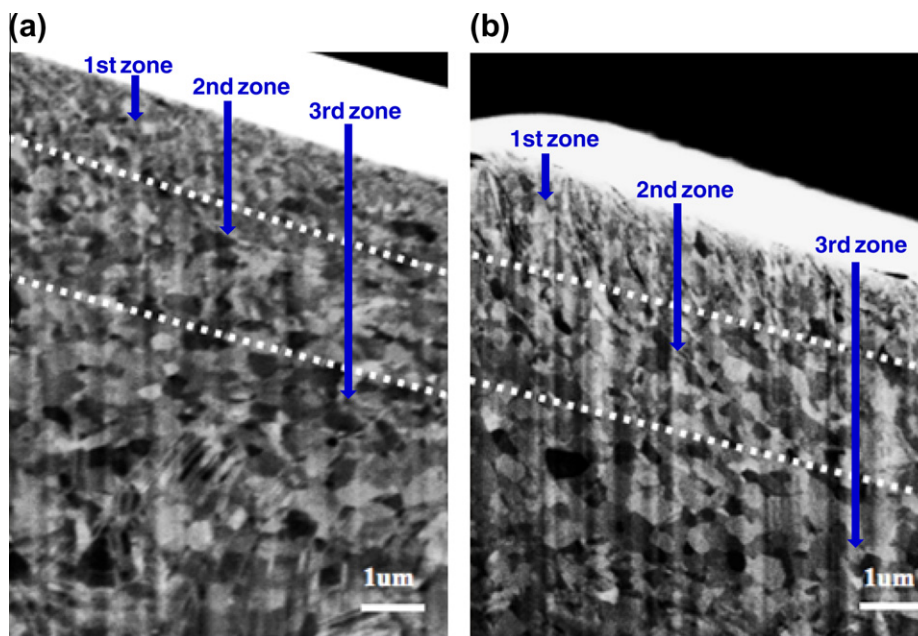


Fig. 6. Comparison of SEM images of (a) LDNT Cu and (b) HDNT Cu just below the scratch surface after 82 passes of sliding. The images show that after repeated contact sliding, both specimens have similar microstructure in the vicinity of the scratch.

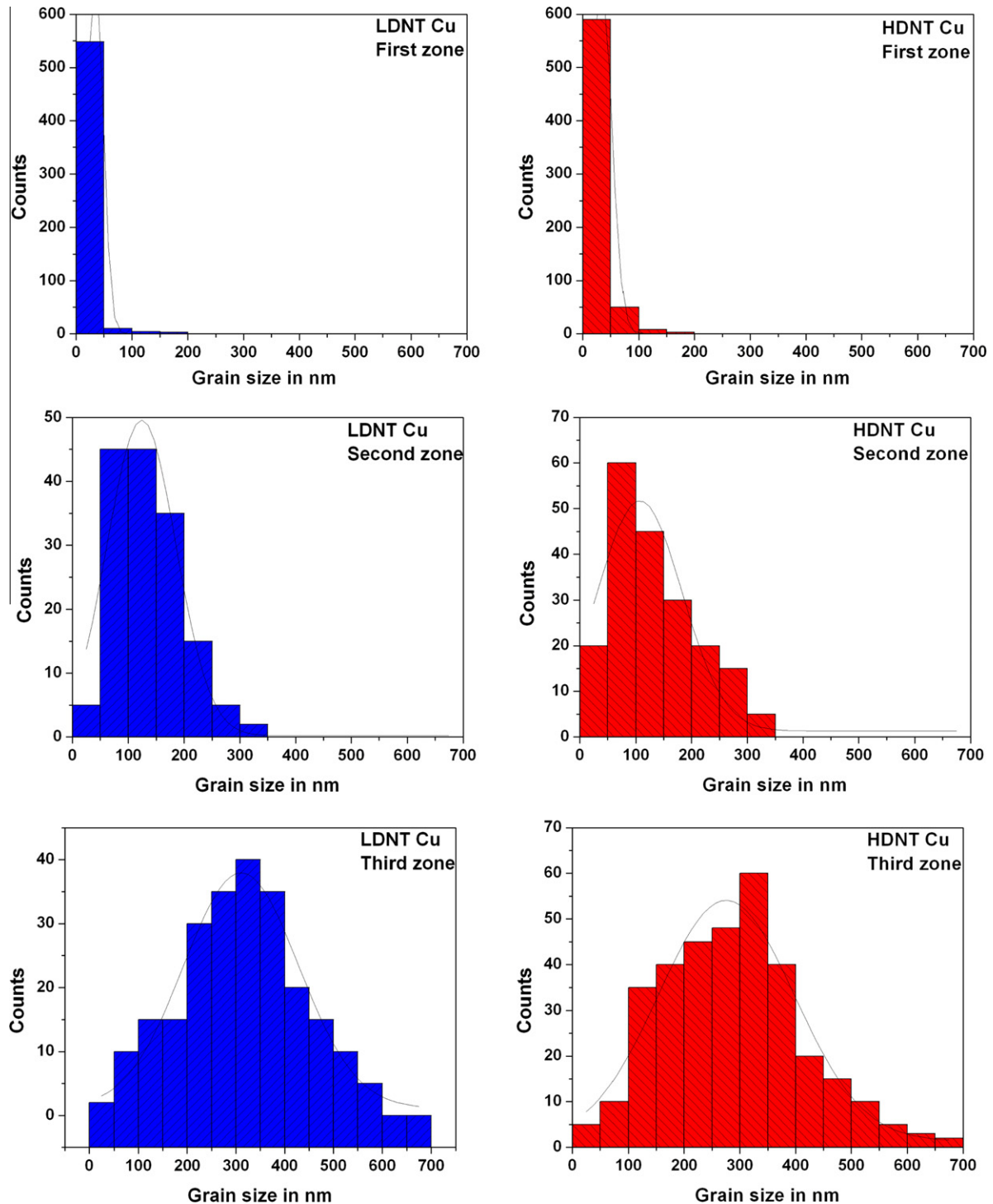


Fig. 7. Plots of grain size distribution after 82 passes of sliding within the three deformation zones in LDNT Cu and HDNT Cu. It can be seen that grain size distributions for both LDNT and HDNT Cu are very similar in all three deformation zones.

dynamically evolving tribolayer and not by the initial microstructure alone.

Prior work has examined the individual contributions of hardness and grain size to the evolution of friction coefficient in Cu during surface scratching experiments by varying the strength through cold working and annealing while

keeping the grain size values relatively constant (with average grain size of 340 and 420 nm, respectively) [18]. For the case of monotonic sliding, these experiments suggest that hardness has a stronger effect on friction coefficient, and that the friction coefficient decreases with an increase in strength. The present study is consistent with

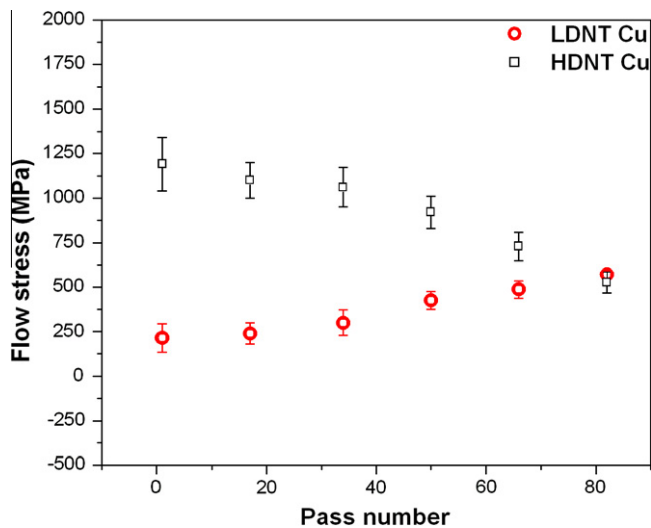


Fig. 8. Estimated surface flow stress of HDNT and LDNT Cu specimens as a function of sliding passes obtained by indentation within the sliding tracks up to 1  $\mu\text{m}$  deep. The LDNT specimen hardens with an increase in the number of sliding cycles as a result of deformation-induced microstructure changes, whereas the HDNT specimen softens. The flow stress close to the surface of the specimens after 82 sliding passes is similar for both specimens.

that observation as the friction coefficient was shown to decrease after the first pass of sliding with an increase in hardness that was in turn controlled by twin density.

Repeated sliding experiments performed on structural ceramics indicate that friction evolution is determined by the force required to initiate deformation (this includes plastic deformation and fracture), and by the force needed to counter the adhesive force generated between the diamond tip and the surrounding material [31]. For the case of ductile NT Cu, on the other hand, it is evident from the present study that the amount of material ploughed by the indenter can also be a critical factor among other factors, such as evolving microstructure, adhesion between the tip and the material and the changing geometry of the groove, in determining the total friction coefficient as the indenter has to bear the tangential load of moving the ploughed material forward or piling it along the sides. In addition, the substrate material also undergoes structural evolution in response to severe deformation. Here, the total friction coefficient decreases with pass number as the material ploughed by the indenter (measured by pile-up height increase per pass) decreases. After successive passes, we observe a constant rate of pile-up height increase and a steady friction coefficient. This trend appears to emerge as the material underneath the scratch acquires a steady-state microstructure that does not change with subsequent sliding cycles.

Grain size and twin lamellar spacing are the two key length scales that characterize structure evolution. In the present study, microscopic observations of the area below the first scratch for LDNT Cu after the 1st scratch pass (Fig. 4a) reveal that grain refinement into the nanoscale regime occurs in the first zone. The variation of the strain

and strain rate of deformation with an increase in depth below the indenter leads to a gradient in the microstructure: the grain size becomes coarser with depth, from  $\sim 30$  nm close to the scratch surface to  $\sim 400$  nm at a depth of 3  $\mu\text{m}$  below the surface. Therefore, close to the scratch surface for LDNT Cu, there occurs significant grain refinement with respect to the original grain size of 450 nm, while there is a simultaneous evolution of structure refinement and gradation with respect to the original twin lamellar spacing ( $\lambda \sim 85$  nm). (This is because the evolved grain size is smaller than 85 nm closer to the surface but larger than 85 nm at greater depths below the surface.)

Processing methods such as cold rolling, equal channel angular pressing (ECAP), surface mechanical attrition treatment (SMAT) and dynamic plastic deformation (DPD) [1,19,32] purposely impose grain refinement by facilitating excessive dislocation activity through high plastic strains. In these cases, grain refinement occurs through dislocation entanglement under the high stresses/strains. The resulting structure subsequently rearranges spatially so as to relieve stored elastic energy by forming substructures such as cells and cell-blocks with a high concentration of dislocations at the cell walls but leaving the cell interior relatively dislocation free [33–35]. The misorientation between adjacent cell-blocks increases with increasing strain and the average size of the cells becomes smaller. Grain refinement via dislocation processes is achieved when these cell walls eventually transform to high-angle boundaries. Grain refinement via initial twin lamellae formation and subsequent dislocation–twin interactions has also been observed during the SMAT process within the top surface layer of CG Cu [36]. The minimum size of these grains has been observed to be close to 10 nm. Initial microstructure refinement is likely to have taken place by dislocation rearrangements; however, with further grain refinement dislocation activity would be suppressed and deformation is speculated to be occurring via twins at the higher strain rates in the layer close to the surface. Molecular dynamics simulations of the deformation of NT Cu [37] have shown full and partial dislocation emission from the grain boundaries (GBs), TB migration (TBM), partial dislocation–TB interaction and formation of twinning faults as some of the microscopic deformation processes. In addition, higher deformation builds up an excessive number of dislocations that interact with TBs and may result in TBs losing coherence [38] and in the breakdown of most of the TBs. High-pressure torsion (HPT) studies on UFG Cu–30 wt.% Zn [39] suggest that, due to a decrease in the stacking fault energy of Cu by alloying with Zn, there is an increased propensity for deformation via twinning rather than via dislocation processes leading to the formation of twin lamellae of thickness  $\sim 13$  nm through partial emission of dislocations from the GBs. Transmission electron microscopy (TEM) observations [40] have shown that newly formed GBs serve as sites for the emission of partial dislocations and the formation of secondary deformation twins; the intersection of these

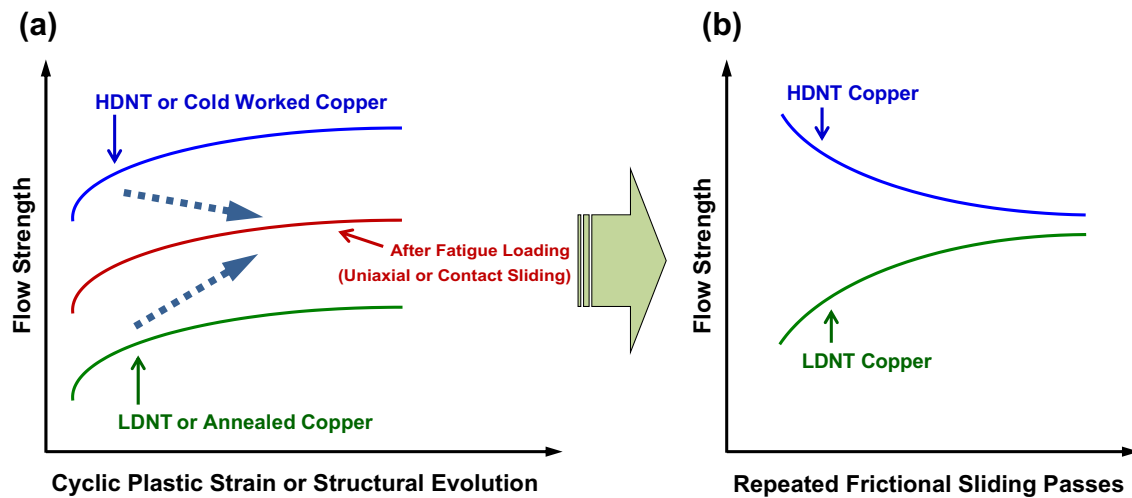


Fig. 9. A schematic drawing of the flow strength evolution as a function of the cyclic plastic strain imposed. A convergence of the final structure and flow strength is observed for different initial microstructures and load histories after repeated cycles of loading for both uniaxial tension/compression and frictional contact [27,28,47].

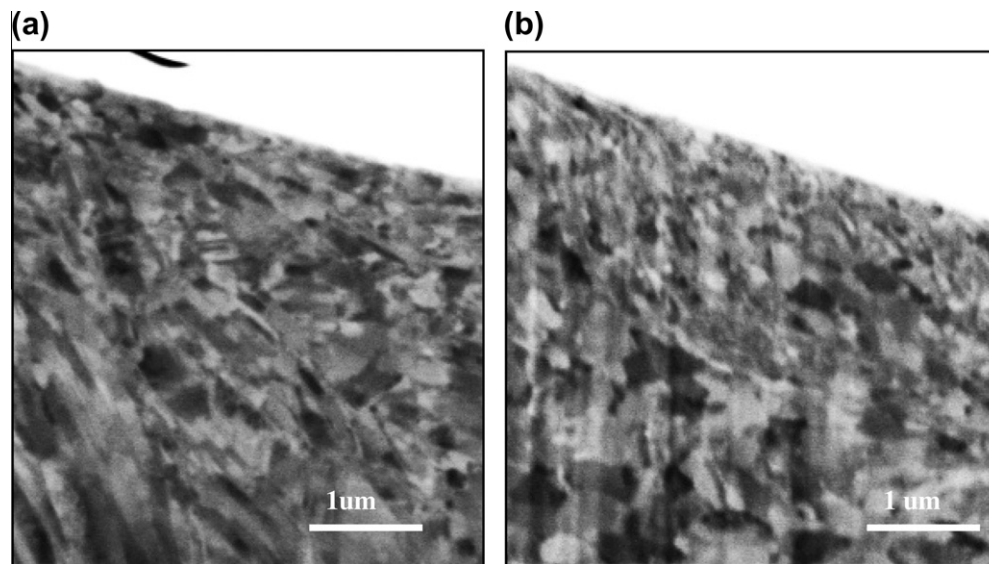


Fig. 10. Close-up SEM observations of the region just below the scratch surface for LDNT Cu (a) after the 1st pass (b) after the 82nd pass. Grain refinement occurs close to the surface after the 1st pass of sliding and can be attributed to dislocation manipulation, rearrangement and twinning processes. After the 82nd pass the deformation-affected zone expands and the grain size distribution conforms to the strain and strain rates beneath the scratch.

twins and the new GBs can lead to the formation of smaller cell blocks within the twin lamellae, leading to microstructure refinement even across the larger dimension of the twin lamellae parallel to the TBs. These newly formed TBs are transformed into high-angle GBs and grain refinement can be achieved after dislocation interactions with the new TBs and possible grain rotations [41,42].

In light of these previous studies, it is conceivable that under the imposed high strains, deformation occurs by twinning in addition to dislocation processes due to the moderate stacking fault energy of Cu. Nanotwins have also been observed in the tribolayer in earlier wear studies [43,44]. Processes such as new twin lamellae formation,

dislocation–TB interaction, TB migration, detwinning of TBs, transformation of TBs into high-angle GBs as well as the formation of dislocation blocks inside twin lamellae could play a major role in deformation and grain-refinement processes [36,43,44].

No obvious change in grain size could be seen for the case of HDNT Cu specimen after the first sliding pass (Fig. 4b). This may be attributed to the high density of TBs that not only curtail GB motion but also store significant plastic strain by accommodating large numbers of dislocations along the TBs. Stability of the NT structure in Cu under severe conditions of localized stresses has also been previously reported [21,22].

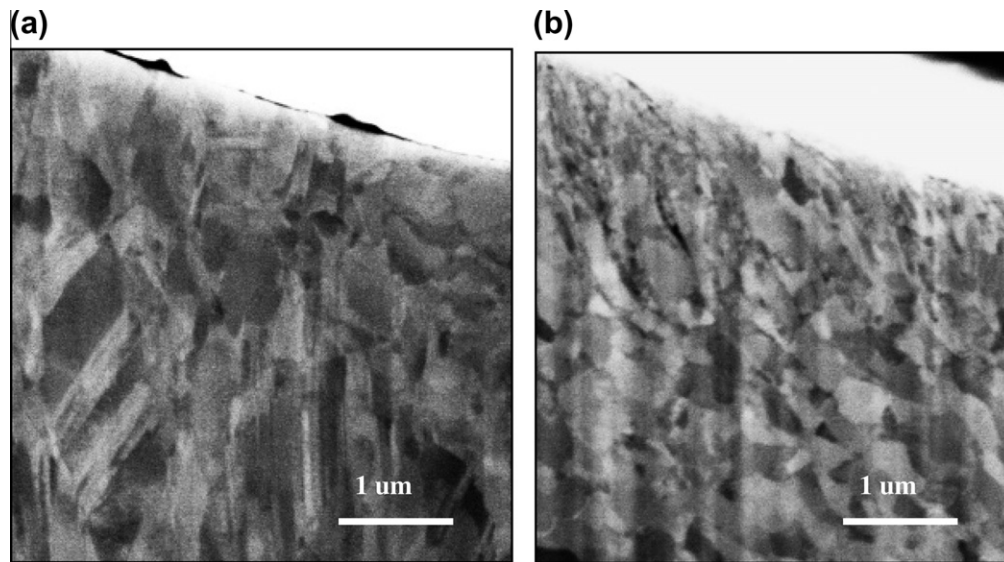


Fig. 11. Close-up SEM observations of the region just below the scratch surface for HDNT Cu (a) after the 1st pass and (b) after the 82nd pass. The microstructure after the 1st pass is not severely affected as most of the plastic deformation can be accommodated by the high density/area of twin boundaries. However, after the 82nd pass, grain refinement occurs, possibly via dislocation rearrangements and twinning processes.

After 82 passes, there is significant refinement in LDNT Cu over a much larger region than after the 1st pass with the grain size progressively increasing with the distance from the surface. No significant structure change is evident after the 1st pass in HDNT Cu. However, after 82 passes the grain size distribution for HDNT Cu is similar to that for LDNT Cu as can be seen in Figs. 6 and 7. The minimum grain size is clearly lower than 30 nm along the scratch surface for both LDNT and HDNT Cu after 82 passes, which is approaching the finest grain size ( $\sim 10$  nm) obtained after high-strain-rate SMAT processes in Cu [36]. The transformation of LDNT Cu and HDNT Cu to a similar microstructure, however, was achieved only after many repeated passes of sliding and not after the 1st pass in spite of the similar values of high stresses/strains imposed beneath the indenter in both cases. This underscores the significance of repeated contact sliding with the attendant possibility of accumulated interactions of dislocations and TBs, and their simultaneous rearrangements such that the final microstructure is dependent solely on accumulated strains, and not on the initial twin density.

The effect of the drastic change in the microstructure of the specimens subsequent to repeated sliding is also evident in the strength evolution of the material just beneath the scratch surface. After the first pass, there is significant grain refinement close to the surface in LDNT Cu. When a  $1 \mu\text{m}$  deep indentation is made (within the grooved scratch scar), the indenter sampled grains with an average grain size of  $\sim 180$  nm and the measured flow stress was close to 200 MPa. This suggests a possible absence of nanoscale twins in the newly formed grains since a significantly higher flow stress would be expected if there were nanoscale twins inside the nanograins. Further, the flow stress evolution in LDNT Cu with the number of passes shows that the

strength of the material increases with the increase in the number of sliding passes. This could possibly arise due to the increase in grain refinement with an increase in the number of sliding cycles.

The average surface flow stress estimated via indentation after the 1st sliding pass in HDNT Cu is  $\sim 1$  GPa. This is because the region in the vicinity of the scratch still retains the NT microstructure. It can be seen in Fig. 8 that HDNT has high flow stress to begin with, but softens to a similar value of flow stress ( $\sim 670$  MPa) as does LDNT Cu after 82 passes of sliding. The average size of the grains sampled during indentation in this case was  $\sim 40$ – $50$  nm. This is consistent with the observations [45] in which the flow stress for NG Cu with an average grain size of 54 nm was reported to be 680 MPa. However, the final grain size sampled by the indenter after 82 passes is larger than the initial smallest microstructural length scale of 15 nm leading to a softening of HDNT Cu.

The above observation of Cu with different initial microstructures converging eventually to the same strength and microstructure after multiple cycles of contact sliding mirrors trends long known from traditional uniaxial, strain-controlled fatigue experiments (see Fig. 9). Mechanical fatigue of fcc metals with high stacking fault energy but with different loading histories and microstructures has been shown to produce similar steady-state saturation flow strength after repeated uniaxial strain fatigue cycles [27,28]. This steady-state microstructure is independent of the prior loading history and is solely dependent on the temperature, strain rate and specific amplitude and kind of stresses and strains just below the indenter. This convergence of microstructure is due to the high stacking fault energy of metals, which promotes significant cross-slip for the formation of a cell structure irrespective of the initial microstructure. Both

dislocation processes and twinning mechanisms can operate in Cu because it has a medium stacking fault energy ( $40 \times 10^{-3} \text{ J m}^{-2}$ ) [46]. The dominant mechanism would depend on strain, strain rate and temperature. This is evident in Fig. 6, where after 82 passes of sliding a gradient in microstructure is evident. This gradient is dependent on the strain rate and strain but not on the initial twin density. Pure fcc metals harden or soften to a steady-state saturation stress and microstructure, after an initial transient regime, under uniaxial strain-controlled fatigue. The steady-state microstructure attained after multiple contact sliding cycles after transient phases of the evolution of friction and material pile-up also demonstrates a similar shake-down flow stress during contact fatigue.

## 5. Conclusions

The wear response of UFG Cu having different twin lamellae thicknesses was examined under monotonic and repeated contact sliding. The major findings of this work are as follows:

- An increase in twin density results in smaller pile-up height and friction coefficient values. With the increase in the number of sliding passes, the total friction coefficient and rate of increase of pile-up for all specimens reach a steady value that does not change significantly in subsequent passes.
- We demonstrate distinct differences between the effects of monotonic and repeated frictional sliding on the deformation-induced microstructure evolution. HDNT Cu exhibited structural stability against the high stresses and strains beneath the indenter after the 1st pass of sliding. This is in contrast to LDNT Cu, which undergoes grain refinement in the vicinity of the scratch just after the 1st pass. However, after 82 passes of sliding, we observe that both LDNT and HDNT Cu exhibit significant microstructure changes and the grain size distribution varies with the depth below the scratch. The finest grain size observed ( $<30 \text{ nm}$ ) is close to the finest grain size observed in repeated sliding of CG Cu and also for SPD processes such as SMAT and HPT in which twinning processes operate in addition to dislocation activities.
- A combination of dimensional analysis and parametric FEM simulations was used to obtain the analytical expression of the curvature of the load ( $P$ ) vs. displacement ( $h$ ) curve when indenting a grooved surface; this can be used to extract elastoplastic properties in the vicinity of the scratch made by a  $70.3^\circ$  conical tip once the experimentally obtained  $P$ – $h$  curve of the indentation on the grooved scratch surface is available.
- The surface hardness evaluated using a  $1 \mu\text{m}$  deep indentation within the scratch grooves for both LDNT and HDNT Cu was also found to be similar after the 82nd pass. This trend follows the well-known result from uni-

axial cyclic straining of high stacking fault energy metals that cold-worked and annealed specimens converge to the same steady-state hardness after multiple cycles. The fact that LDNT specimens showed a considerable increase in hardness with repeated sliding has applications in materials design.

## Acknowledgments

The authors acknowledge financial support by the ONR Grant N00014-08-1-0510. S.S. and M.D. further acknowledge support from the Advanced Materials for Micro and Nano Systems Programme of the Singapore-MIT Alliance (SMA). L.L. acknowledges financial support from the National Science Foundation of China (Grant Nos. 50725103, 50890171 and 51071153), Most International S&T Cooperation Project of China (S2011ZR0270) and the Danish National Research Foundation and the National Natural Science Foundation of China (Grant No. 50911130230) for the Danish-Chinese Center for Nanometals. The authors are grateful to Professor Christopher Schuh at MIT for the insightful discussions on the wear of materials. Mr. S. Jin's help with sample preparation and Dr. J. Tan's help in FIB cutting and SEM observations are also greatly appreciated.

## Appendix A. Extracting plastic properties from indentation on a grooved scratch surface

Since most of the analytical studies in the literature relating indentation data to elastoplastic properties are for the case of indenting a flat surface [48,49], to evaluate the surface material properties after a single scratch test or repeated scratch tests we need to develop a new algorithm to extract plastic properties for the case of indenting a grooved surface. The general-purpose FEM package ABAQUS (SIMULIA, Providence, RI, USA) was used to construct a full three-dimensional model of the indented material and the indenter. Fig. A1 shows the finite-element model set-up for this study. The specimen was modeled using 6000 eight-noded linear brick elements and mesh biasing was done to ensure a finer mesh close to the region where the indenter makes contact with the specimen, as can be seen in Fig. A1c and d. A minimum of 20 elements were in contact with the indenter at the maximum load in each FEM computation. The mesh was determined to be insensitive to the far-field boundary conditions. The diamond indenter was modeled as a rigid body cone with a half-included angle of  $70.3^\circ$  and the contact between the indenter and the specimen was specified as frictionless.

Parametric FEM simulations were performed for elastic–perfectly plastic materials with Young's modulus and yield strength covering the range for most pure and alloyed engineering metals, i.e. the Young's modulus  $E$  was varied from 10 to 210 GPa,  $\sigma_y$  from 30 to 3000 MPa and the Poisson ratio  $\nu$  was kept fixed at 0.33.

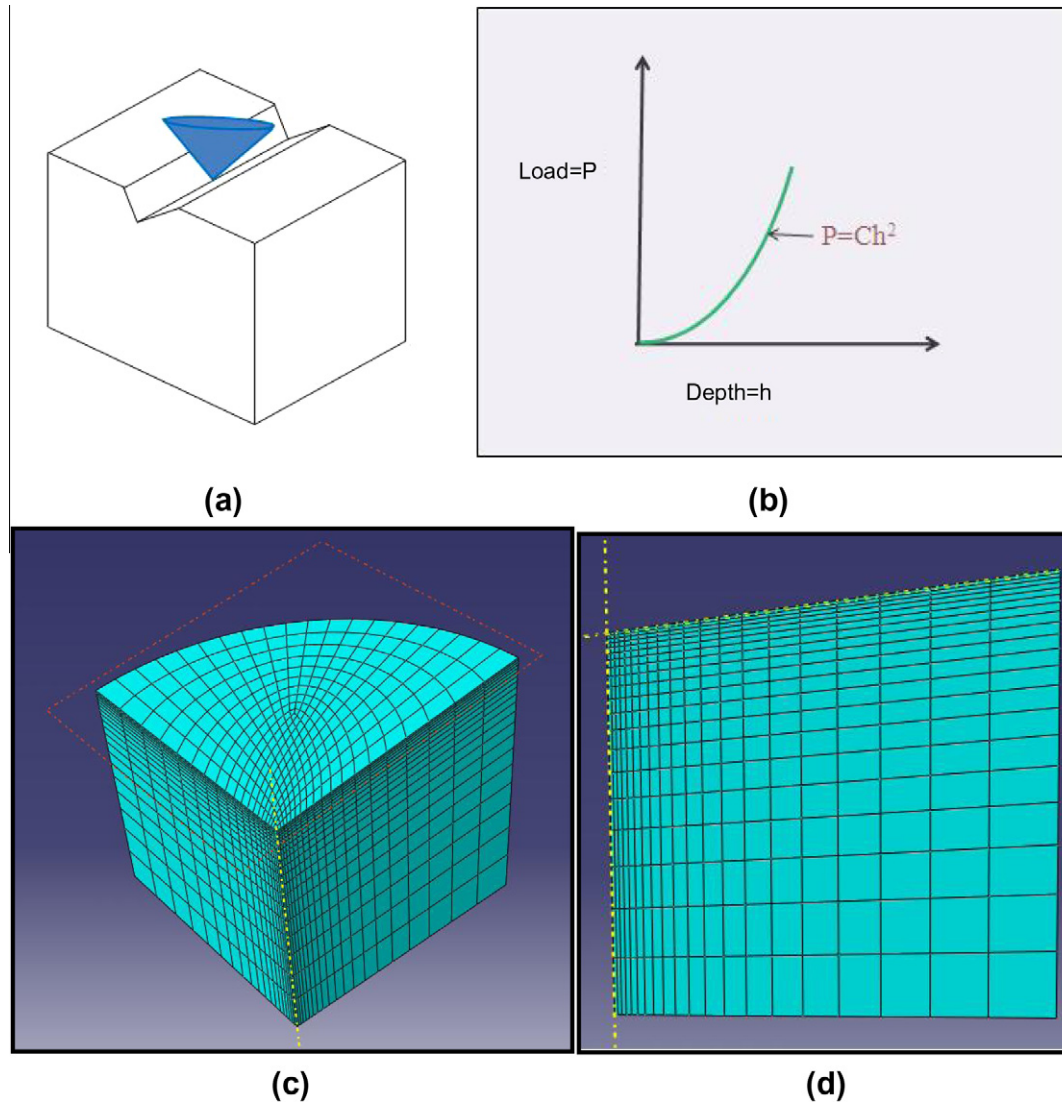


Fig. A1. (a) A schematic drawing of the process of indenting a grooved scratch surface. (b) Typical loading response in the form of a load ( $P$ ) vs. depth ( $h$ ) curve obtained after indenting an elastoplastic material. (c) Isometric view of the FEM mesh design, where the inherent symmetry of the geometries enabled the quarter model construction. (d) Front view of the FEM mesh showing the inclined surface of the specimen being indented.

Dimensional analysis was used to construct functions to relate the loading curvature while indenting a grooved surface as a function of the elastoplastic properties. We followed the general method developed earlier for studying indentation on a flat surface using dimensional analysis and FEM computations [48,49].

For a self-similar sharp indentation test, the load ( $P$ ) required for a conical indenter to penetrate a depth ( $h$ ) into an elastic–perfectly plastic material can be written as:

$$P = P(h, E, \nu, \sigma_y, E_i, \nu_i), \quad (\text{A1})$$

where  $E_i$  and  $\nu_i$  are the Young's modulus and Poisson's ratio of the indenter, respectively. The elastic effects of the indenter and material can be incorporated into a single parameter  $E^*$  where:

$$E^* = \left[ \frac{1 - \nu^2}{E} + \frac{1 - \nu_i^2}{E_i} \right]^{-1}. \quad (\text{A2})$$

Using Eq. (A2), Eq. (A1) can be rewritten as:

$$P = P(h, E^*, \sigma_y). \quad (\text{A3})$$

Applying the  $\Pi$  theorem in dimensional analysis, Eq. (A3) can be transformed as:

$$P = \sigma_y h^2 \Pi \left( \frac{E^*}{\sigma_y} \right), \quad (\text{A4})$$

where  $\Pi$  is a dimensionless function. Fig. A1b shows the typical indentation response of an elastoplastic material in terms of the load,  $P$ , required to penetrate depth,  $h$ . The loading curve follows Kick's law  $P = Ch^2$  for a self-similar sharp indentation [48]. Assuming the indentation depth in Fig. A1a is much smaller than the groove depth, the indentation can be considered self-similar and follows Kick's law. The parameter  $C$ , also known as the curvature of the loading curve, can be expressed using Eq. (A4) as:

$$C = \frac{P}{h^2} = \sigma_y \Pi \left( \frac{E^*}{\sigma_y} \right). \quad (\text{A5})$$

For simplicity, here we assume the indentation size effect can be ignored, and consequently  $C$  is a material constant. Eq. (A5) and FEM computations can be used to determine the analytical expression for  $C$  as a function of the elasto-plastic parameters.

A total of 12 cases with different material properties were simulated and the results are shown in Fig. A2 using diamond symbols. Using the same functional form used earlier [48], the following dimensionless function can be extracted by fitting the simulation data points:

$$\begin{aligned} \Pi = \frac{C}{\sigma_y} = & -2.208 \left[ \ln \left( \frac{E^*}{\sigma_y} \right) \right]^3 + 29.45 \left[ \ln \left( \frac{E^*}{\sigma_y} \right) \right]^2 \\ & - 81.21 \left[ \ln \left( \frac{E^*}{\sigma_y} \right) \right] + 92.53. \end{aligned} \quad (\text{A6})$$

The values for indenting a flat surface are also plotted here with square symbols in Fig. A2 using the following function, which can be found in Ref. [48]:

$$\begin{aligned} \frac{C}{\sigma_y} = & -1.131 \left[ \ln \left( \frac{E^*}{\sigma_y} \right) \right]^3 + 13.635 \left[ \ln \left( \frac{E^*}{\sigma_y} \right) \right]^2 \\ & - 30.594 \left[ \ln \left( \frac{E^*}{\sigma_y} \right) \right] + 29.267. \end{aligned} \quad (\text{A7})$$

We repeated the computational study of indenting a flat surface and found our results to be in good agreement with the above equation.

It can be concluded by looking at Fig. A2 that indenting a grooved surface offers more resistance than indenting a flat surface. With the known modulus of  $E^*$  and the indentation curvature  $C$  obtained from experiments, the yield strength  $\sigma_y$  can be extracted using Eq. (A6).

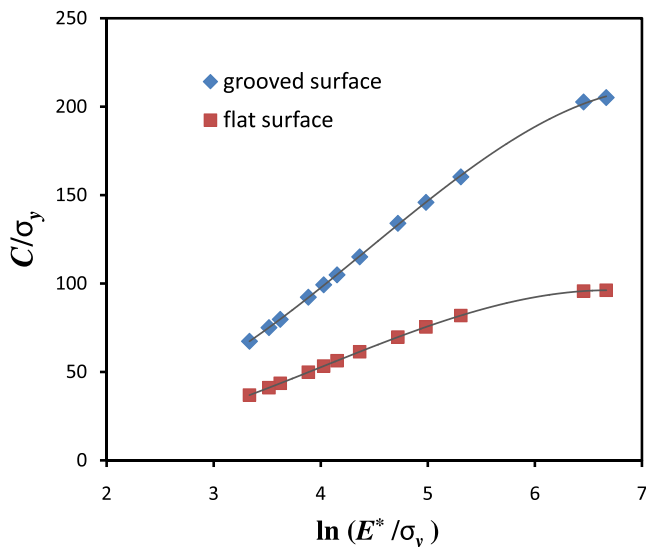


Fig. A2. Dimensionless function  $\Pi = C/\sigma_y$  as a function of  $\ln(E^*/\sigma_y)$  obtained from FEM simulations of indenting a grooved or a flat surface using a conical indenter with a half-included angle of  $70.3^\circ$ .

## References

- [1] Kumar KS, Van Swygenhoven H, Suresh S. Acta Mater 2003;51(19):5743–74.
- [2] Hanlon T, Tabachnikova ED, Suresh S. Int J Fatigue 2005;27(10-12):1147–58.
- [3] Karimpoor AA, Erb U. Phys Stat Solidi A 2006;203(6):1265–70.
- [4] Mirshams RA, Mao CH, Whang SH, Yin WM. Mater Sci Eng A 2001;315(1-2):21–7.
- [5] Zhang X, Misra A, Wang H, Shen TD, Nastasi M, Mitchell TE, et al. Acta Mater 2004;52(4):995–1002.
- [6] Wu BYC, Ferreira PJ, Schuh CA. Metall Mater Trans A 2005;36A:1927–36.
- [7] Lu L, Shen YF, Chen XH, Qian LH, Lu K. Science 2004;304(5669):422–6.
- [8] Anderoglu O, Misra A, Wang H, Ronning F, Hundley MF, Zhang X. Appl Phys Lett 2008;93(8):083108.
- [9] Lu L, Schwaiger R, Shan ZW, Dao M, Lu K, Suresh S. Acta Mater 2005;53(7):2169–79.
- [10] Dao M, Lu L, Shen YF, Suresh S. Acta Mater 2006;54(20):5421–32.
- [11] Lu K, Lu L, Suresh S. Science 2009;324(5925):349–52.
- [12] Singh A, Tang L, Dao M, Lu L, Suresh S. Acta Mater 2011;59:2437–46.
- [13] Christian JW, Mahajan S. Prog Mater Sci 1995;39(1-2):1–157.
- [14] Babyak WJ, Rhines FN. Trans Am Inst Min Metall Eng 1960;218(1):21–3.
- [15] Fan GJ, Wang YD, Fu LF, Choo H, Liaw PK, Ren Y, et al. Appl Phys Lett 2006:88.
- [16] Hong CS, Tao NR, Lu K, Huang X. Scripta Mater 2009;61(3):289–92.
- [17] Dao M, Lu L, Asaro RJ, De Hosson JTM, Ma E. Acta Mater 2007;55(12):4041–65.
- [18] Hanlon T, Chokshi AH, Manoharan M, Suresh S. Int J Fatigue 2005;27(10-12):1159–63.
- [19] Bellemare S, Dao M, Suresh S. Int J Solids Struct 2007;44(6):1970–89.
- [20] Bellemare SC, Dao M, Suresh S. Mech Mater 2008;40(4-5):206–19.
- [21] Shute CJ, Myers BD, Xie S, Barbee TW, Hodge AM, Weertman JR. Scripta Mater 2009;60(12):1073–7.
- [22] Shute CJ, Myers BD, Xie S, Li S-Y, TWB Jr, Hodge AM, et al. Acta Mater 2011;59(11):4569–77.
- [23] Hirth JP, Rigney DA. Wear 1976;39(1):133–41.
- [24] Bhargava RK, Moteff J, Swindeman RW. Metall Trans A 1977;8(5):799–800.
- [25] Rigney DA, Glaeser WA. Wear 1978;46(1):241–50.
- [26] Rupert TJ, Schuh CA. Acta Mater 2010;58(12):4137–48.
- [27] Feltner CE, Laird C. Acta Metall 1967;15(10):1621.
- [28] Feltner CE, Laird C. Acta Metall 1967;15(10):1633.
- [29] Kitsunai H, Kato K, Hokkirigawa K, Inoue H. Wear 1990;135(2):237–49.
- [30] Rigney DA, Naylor MGS, Divakar R, Ives LK. Mater Sci Eng 1986;81(1-2):409–25.
- [31] Gee MG. Wear 2001;250:264–81.
- [32] Li YS, Tao NR, Lu K. Acta Mater 2008;56(2):230–41.
- [33] Liu Q, Jensen DJ, Hansen N. Acta Mater 1998;46(16):5819–38.
- [34] Wang YB, Liao XZ, Zhu YT. Int J Mater Res 2009;100(12):1632–7.
- [35] Ungar T, Gubicza J, Ribarik G, Borbely A. J Appl Crystallogr 2001;34:298–310.
- [36] Wang K, Tao NR, Liu G, Lu J, Lu K. Acta Mater 2006;54(19):5281–91.
- [37] Shabib I, Miller RE. Modell Simulat Mater Sci Eng 2009;17(5):055009.
- [38] Zhu T, Li J, Samanta A, Kim HG, Suresh S. Proc Natl Acad Sci U S A 2007;104(9):3031–6.
- [39] Wang YB, Liao XZ, Zhao YH, Lavernia EJ, Ringer SP, Horita Z, et al. Mater Sci Eng A 2010;527(18-19):4959–66.
- [40] Wang YB, Wu B, Sui ML. Appl Phys Lett 2008;93(4):041906.
- [41] Ke M, Hackney SA, Milligan WW, Aifantis EC. Nanostruct Mater 1995;5(6):689–97.

- [42] Wang YB, Li BQ, Sui ML, Mao SX. *Appl Phys Lett* 2008;92(1):011903.
- [43] Singh JB, Cai W, Bellon P. *Wear* 2007;263:830–41.
- [44] Singh JB, Wen JG, Bellon P. *Acta Mater* 2008;56(13):3053–64.
- [45] Cheng S, Ma E, Wang YM, Kecskes LJ, Youssef KM, Koch CC. *Acta Mater* 2005;53(5):1521–33.
- [46] Komura S, Horita Z, Nemoto M. *J Mater Res* 1999;14(10):4044–50.
- [47] Suresh S. *Fatigue of materials*. 2nd ed. Cambridge: Cambridge University Press; 1998.
- [48] Dao M, Chollacoop N, Van Vliet KJ, Venkatesh TA, Suresh S. *Acta Mater* 2001;49(19):3899–918.
- [49] Gouldstone A, Chollacoop N, Dao M, Li J, Minor AM, Shen YL. *Acta Mater* 2007;55(12):4015–39.